Solitonic Josephson Thermal Transport

Claudio Guarcello,[1,2,*] Paolo Solinas,[3] Alessandro Braggio,[1] and Francesco Giazotto[1]

[1]*NEST, Istituto Nanoscienze-CNR and Scuola Normale Superiore, Piazza San Silvestro 12, I-56127 Pisa, Italy*

[2]*Radiophysics Department, Lobachevsky State University, Gagarin Avenue 23, 603950 Nizhni Novgorod, Russia*

[3]*SPIN-CNR, Via Dodecaneso 33, 16146 Genova, Italy*

(Received 30 November 2017; published 19 March 2018)

We explore the coherent thermal transport sustained by solitons through a long Josephson junction as a thermal gradient across the system is established. We observe that a soliton causes the heat current through the system to increase. Correspondingly, the junction warms up in conjunction with the soliton, with temperature peaks up to, e.g., approximately 56 mK for a realistic Nb-based proposed setup at a bath temperature $T_{\rm bath} = 4.2$ K. The thermal effects on the dynamics of the soliton are also discussed. Markedly, this system inherits the topological robustness of the solitons. In view of these results, the proposed device can effectively find an application as a superconducting thermal router in which the thermal transport can be locally mastered through solitonic excitations, whose positions can be externally controlled through a magnetic field and a bias current.

DOI: 10.1103/PhysRevApplied.9.034014

I. INTRODUCTION

The physics of coherent excitations has relevant implications in the field of condensed matter. Such coherent objects emerge in several extended systems and are usually characterized by remarkable particlelike features. In recent decades, these notions have played a crucial role for understanding various issues in different areas of the physics of continuous and discrete systems [1,2]. A Josephson junction (JJ) is a model system to appreciate coherent excitations, and, specifically, a superconductor-insulator-superconductor (*S*-*I*-*S*) long JJ (LJJ) is the prototypal solid-state environment to explore the dynamics of a peculiar kind of solitary wave called a soliton [3,4]. These excitations give rise to readily measurable physical phenomena, such as step structures in the *I*-*V* characteristic of LJJs and microwave radiation emission. Moreover, a soliton has a clear physical meaning in the LJJ framework since it carries a quantum of magnetic flux, induced by a supercurrent loop surrounding it, with the local magnetic field perpendicularly oriented with respect to the junction length [5]. Thus, solitons in the context of LJJs are usually referred to as fluxons or Josephson vortices. Measured for the first time more than 40 years ago [6,7], LJJs remain an active research field [8–26]. Indeed, the fact that a single topologically protected excitation, i.e., a flux quantum, can be moved and controlled by bias currents, created by the magnetic field, manipulated through shape engineering [9,27–30], or pinned by inhomogeneities [31,32] naturally has stimulated a profusion of ideas and applications.

Practically, several electric and magnetic features concerning solitons in LJJs have hitherto been comprehensively explored, but little is known about the soliton-sustained coherent thermal transport through a temperature-biased junction. This issue falls into the emerging field of coherent caloritronics [33–35], which deals with the manipulation of heat currents in mesoscopic superconducting devices. Here, the aim is to design and realize thermal components able to master the energy transfer with a high degree of accuracy. In this regard, we propose laying the foundation of an alternative branch of fast coherent caloritronics based on solitons, with the end being to build up alternative devices exploiting this highly controllable, phase-coherent thermal flux. Specifically, the feasibility of using a LJJ as a thermal router [36], in which thermal transport can be locally handled through solitonic excitations, is very promising.

After Maki and Griffin's prediction about it in 1965 [37], only recently has phase-coherent thermal transport in temperature-biased Josephson devices been confirmed experimentally in several interferometerlike structures [38–43]. The thermal modulation induced by the external magnetic field was demonstrated in superconducting quantum-interference devices (SQUIDs) [38,39] and short JJs [40,41]. Furthermore, in LJJs, the heat-current diffraction patterns in the presence of an in-plane external magnetic field have been discussed theoretically [44]. However, until now, no efforts have been made to explore how thermal transport across a LJJ is influenced by solitons eventually

*claudio.guarcello@nano.cnr.it

set along it. Nonetheless, it has been demonstrated theoretically that the presence of a fluxon threading a temperature-biased inductive SQUID modifies thermal transport and affects the steady temperatures of a floating electrode of the device [45,46]. Similarly, we demonstrate theoretically that a fluxon arranged within a LJJ locally affects, in a fast time scale, the thermal evolution of the system, and, at the same time, we discuss how the temperature gradient affects the soliton dynamics. Finally, being solitons, namely, remarkably stable and robust objects [47], at the core of its operation, this system provides an intrinsic topological protection on thermal transport.

The paper is organized as follows. In Sec. II, the theoretical background used to describe the phase evolution of a magnetically driven LJJ is discussed. In Sec. III, the thermal balance equation and the heat currents are introduced. In Sec. IV, the evolution of the temperature of the floating electrode is studied as a thermal gradient across the system is taken into account. In Sec. V, conclusions are drawn.

II. PHASE DYNAMICS

In Fig. 1(a), a long and narrow *S-I-S* Josephson junction, in the so-called overlap geometry formed by two superconducting electrodes S_1 and S_2 separated by a thin layer of insulating material with thickness d, is represented. We consider an extended junction with both the length and the width larger than d (namely, $W, L \gg d$). In the geometry depicted in Fig. 1, the junction area $A = WL$ extends into the x-z plane, the electric bias current is eventually flowing in the y direction, and the external magnetic field is applied in the z direction. The thickness of each superconducting electrode is assumed to be larger than the London penetration depth $\lambda_{L,i}$ of the electrode material. Since the applied field penetrates the superconducting electrodes up to a thickness given by the London penetration depth, an effective magnetic thickness of the junction $t_d = \lambda_{L,1} + \lambda_{L,2} + d$ can be defined. If $\lambda_{L,i}$ values are larger than the thickness of the electrodes D_i, the effective magnetic thickness has to be replaced by $\tilde{t}_d = \lambda_{L,1}\tanh(D_1/2\lambda_{L,1}) + \lambda_{L,2}\tanh(D_2/2\lambda_{L,2}) + d$ [40,41]. In the presence of an external in-plane magnetic field $\mathbf{H}(\mathbf{r},t) = (0,0,-H(t)\hat{\mathbf{z}})$, the phase φ—namely, the phase difference between the wave functions describing the carriers in the superconducting electrodes—changes according to $\partial\varphi(x,t)/\partial x = [(2\pi)/(\Phi_0)]\mu_0 t_d H(t)$ [48], where $\Phi_0 = h/2e \simeq 2\times10^{-15}$ Wb is the magnetic flux quantum (with e and h being the electron charge and the Planck constant, respectively), and μ_0 is the vacuum permeability. For a long and narrow junction, we assume that $W \ll \lambda_J$ and $L \gg \lambda_J$, where we introduce the length scale $\lambda_J = \sqrt{[\Phi_0/(2\pi\mu_0)][1/(t_d J_c)]}$, called the *Josephson penetration depth*, where $J_c = I_c/A$ is the critical current area density. Then, in normalized units, the linear dimensions of the junction read $\mathcal{L} = L/\lambda_J \gg 1$ and $\mathcal{W} = W/\lambda_J \ll 1$.

The electrodynamics of a LJJ is usually described by a partial differential equation for the order-parameter phase difference φ—namely, the perturbed sine-Gordon (SG) equation—that, in the normalized units $\tilde{x} = x/\lambda_J$ and $\tilde{t} = \omega_p t$, with $\omega_p = \sqrt{[(2\pi)/\Phi_0](I_c/C)}$ being the *Josephson plasma frequency* [48], reads [48,49]

$$\frac{\partial^2\varphi(\tilde{x},\tilde{t})}{\partial\tilde{x}^2} - \frac{\partial^2\varphi(\tilde{x},\tilde{t})}{\partial\tilde{t}^2} - \sin[\varphi(\tilde{x},\tilde{t})] = \alpha\frac{\partial\varphi(\tilde{x},\tilde{t})}{\partial\tilde{t}}. \quad (1)$$

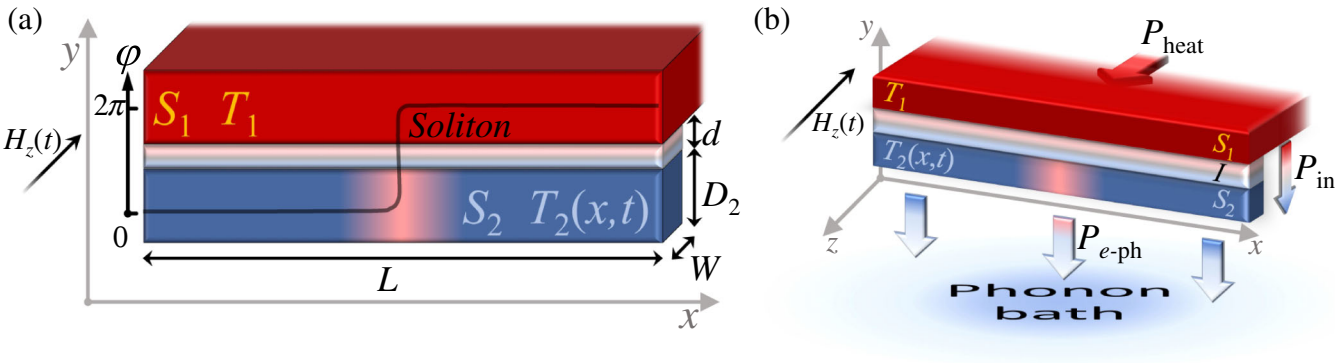

FIG. 1. (a) A *S-I-S* rectangular LJJ excited by an external in-plane magnetic field $H_z(t)$. The length and the width of the junction are $L \gg \lambda_J$ and $W \ll \lambda_J$, respectively, where λ_J is the Josephson penetration depth. Moreover, the thickness $D_2 \ll \lambda_J$ of the electrode S_2 is indicated. A soliton within the junction, corresponding to a 2π twist of the phase φ, is represented. T_i is the temperature of the superconductor S_i, and d is the insulating layer thickness. (b) Thermal model of the device as the thermal contact with a phonon bath is taken into account. The heat current, $\mathcal{P}_{in}$, flowing through the junctions depends on the temperatures and the solitons eventually set along the system. $P_{e\text{-ph}}$ represents the coupling between quasiparticles in S_2 and the lattice phonons residing at T_{bath}, whereas P_{heat} denotes the power injected into S_1 through heating probes in order to impose a fixed quasiparticle temperature T_1. The arrows indicate the direction of the heat currents for $T_1 > T_2 > T_{bath}$.

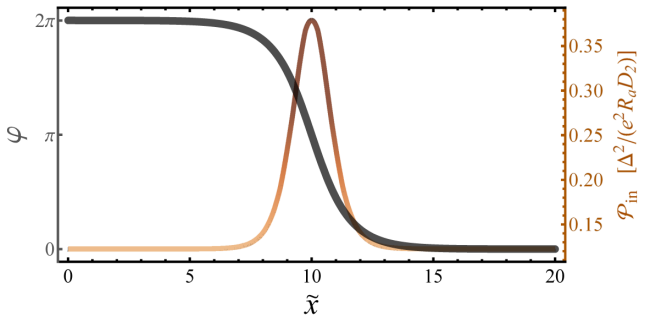

FIG. 2. The phase profile φ (left vertical scale, the black line) and the heat power density $\mathcal{P}_{\rm in}(T_1, T_2, \varphi)$ [in units of $\Delta_2^2(0)/(e^2R_aD_2)$] (right vertical scale, the orange line)—see Eq. (7)—for $T_1 = 7$ K and $T_2 = 4.2$ K, as a function of the normalized position $\tilde{x}$, when a steady unperturbed soliton [see Eq. (3) for $u = 0$] is located at the midpoint of a junction with normalized length $\mathcal{L} = 20$.

The boundary conditions of this equation take into account the normalized external magnetic field $\mathcal{H}(t) = [(2\pi)/(\Phi_0\mu_0)]t_d\lambda_J H(t)$:

$$\frac{d\varphi(0,t)}{d\tilde{x}} = \frac{d\varphi(L,t)}{d\tilde{x}} = \mathcal{H}(t). \tag{2}$$

In Eq. (1), $\alpha = (\omega_p RC)^{-1}$ is the damping parameter (with R and C being the total normal resistance and capacitance of the JJ).

The SG equation admits topologically stable traveling-wave solutions, called *solitons* [3,4], corresponding to 2π twists of the phase (see Fig. 2). For the unperturbed SG equation, i.e., $\alpha = 0$ in Eq. (1), solitons have the simple analytical expression [48]

$$\varphi(\tilde{x} - u\tilde{t}) = 4\arctan\left[\exp\left(\pm\frac{(\tilde{x} - \tilde{x}_0 - u\tilde{t})}{\sqrt{1-u^2}}\right)\right], \tag{3}$$

where the sign $\pm$ is the polarity of the soliton and u is the soliton speed normalized to the Swihart velocity [48], namely, the largest group propagation velocity of the linear electromagnetic waves in long junctions. The moving soliton corresponds to a time variation of the phase which generates a local voltage drop according to $V(x,t) = \Phi_0/(2\pi)\dot{\varphi}(x,t)$.

For the numerical simulation of the soliton dynamics, we modeled the normalized external magnetic field $\mathcal{H}(t)$ as a Gaussian pulse exciting the junction end in $x = 0$. Accordingly, the boundary conditions become

$$\frac{d\varphi(0,t)}{d\tilde{x}} = \mathcal{H}(t) \quad \text{and} \quad \frac{d\varphi(L,t)}{d\tilde{x}} = 0. \tag{4}$$

For simplicity, in our model, i.e., Eq. (1), both of the terms $\beta[(\partial\varphi)/(\partial\tilde{x}^2\partial\tilde{t})]$ [3,49] (with $\beta = \omega_p L_P/R_P$, where $L_P = \mu_0 t_d/W$ and R_P represents the scattering of quasiparticles in the superconducting surface layers) and $\Delta_c[(\partial H)/(\partial\tilde{x})]$ [3,50] (with Δ_c being a coupling constant) are omitted. These terms account for the dissipation due to the surface resistance of the superconducting electrodes and for the spatial gradient of the magnetic field along the junction, respectively. We neglect these contributions since we are interested only in looking at the interplay between a soliton and the thermal effects resulting from its presence along the system as a temperature gradient across the junction is imposed. In this regard, the specific mechanism used to excite a soliton is also not very relevant. In fact, in place of a moving soliton generated by a magnetic pulse, we can alternatively design the local control of thermal flux through configurations of steady solitons excited in specific points of the junction via a slowly varying external magnetic drive applied to both edges of the device [44]. In this manner, the positions of the solitons are directly dependent on the boundary conditions. Anyway, we observe that, still in this case, a dynamical treatment is crucial for the realistic description of the manipulation of the system, and it leads to peculiar results, such us the hysteresis and the trapping of fluxons [44]. Alternatively, in an annular geometry [51], i.e., a "closed" LJJ folded back into itself in which solitons move undisturbed (i.e., without any interaction with borders), fluxons can be excited at will [52,53], allowing highly controlled soliton dynamics.

Below, we also briefly discuss the possibility of controlling the soliton position with an applied bias current. This feasibility adds an external control knob, making this device more interesting for practical applications.

III. THERMAL EFFECTS

The aim of this section is to explore the thermal flux through the junction, as a soliton is set and a temperature gradient across the junction is imposed. Specifically, we observe the evolution of the temperature $T_2(x,t)$, which depends on all of the energy local relaxation mechanisms occurring in the electrode S_2 [see Fig. 1(b)]. For the sake of simplicity, we assume that the electrode S_1 resides at a fixed temperature T_1, which is maintained by the good thermal contact with heating probes. The electrode S_2 is also in thermal contact with a phonon bath at the temperature $T_{\rm bath} \le T_2 < T_1$.

A characteristic length scale for the thermalization in the diffusive regime can be estimated as the inelastic scattering length $\ell_{\rm in} = \sqrt{D\tau_s}$, where $D = \sigma_N/(e^2N_F)$ is the diffusion constant (with σ_N and N_F being the electrical conductivity in the normal state and the density of states at the Fermi energy, respectively) and τ_s is the recombination quasiparticle lifetime [54]. For Nb at 4.2 K, one obtains $\ell_{\rm in} \sim 0.3$ μm—namely, a value well below the dimension of a soliton, $\ell_{\rm in} \ll \lambda_J$—since $\lambda_J \gtrsim 6$ μm for the device considered below. When only the length of S_2 is much larger than $\ell_{\rm in}$, i.e., $L \gg \ell_{\rm in}$ (namely, the so-called quasiequilibrium limit [33]), the electrode S_2 can be modeled as a one-dimensional diffusive superconductor at a temperature varying along L.

For the sake of readability, hereafter, we adopt in equations the abbreviated notation in which the x and t dependences are left implicit, namely, $T_2 = T_2(x,t)$, $\varphi = \varphi(x,t)$, and $V = V(x,t)$. Then the evolution of the temperature T_2 is given by the time-dependent diffusion equation

$$\frac{d}{dx}\left(\kappa(T_2)\frac{dT_2}{dx}\right) + \mathcal{P}_{\rm tot}(T_1,T_2,\varphi) = c_v(T_2)\frac{dT_2}{dt}, \quad (5)$$

where the rhs represents the variations of the internal energy density of the system and the lhs terms indicate the spatial heat diffusion, taking into account the inhomogeneous electronic heat conductivity, $\kappa(T_2)$, and the total heat flux density in the system, namely,

$$\mathcal{P}_{\rm tot}(T_1,T_2,\varphi) = \mathcal{P}_{\rm in}(T_1,T_2,\varphi,V) - \mathcal{P}_{e\text{-ph},2}(T_2,T_{\rm bath}). \quad (6)$$

This term consists of the incoming, i.e., $\mathcal{P}_{\rm in}(T_1,T_2,\varphi,V)$, and outgoing, i.e., $\mathcal{P}_{e\text{-ph},2}(T_2,T_{\rm bath})$, thermal power densities in S_2. We stress that the phase dynamics is essential, through $\mathcal{P}_{\rm in}$, to determining the heat flows and the temperature evolution. Therefore, Eqs. (1) and (5) both have to be solved numerically self-consistently to thoroughly explore the thermal behavior of the system.

In Eq. (6), the heat current density $\mathcal{P}_{\rm in}(T_1,T_2,\varphi,V)$ flowing from S_1 to S_2 is

$$\mathcal{P}_{\rm in}(T_1,T_2,\varphi,V) = \mathcal{P}_{\rm qp}(T_1,T_2,V) - \cos\varphi\mathcal{P}_{\cos}(T_1,T_2,V) + \sin\varphi\mathcal{P}_{\sin}(T_1,T_2,V), \quad (7)$$

and it contains the interplay between Cooper pairs and quasiparticles in tunneling through a JJ predicted by Maki and Griffin [37]. In fact, $\mathcal{P}_{\rm qp}$ is the heat flux density carried by quasiparticles and represents an incoherent flow of energy through the junction from the hot to the cold electrode [33,37,55]. Instead, the "anomalous" terms $\mathcal{P}_{\sin}$ and $\mathcal{P}_{\cos}$ determine the phase-dependent part of the heat current originating from the energy-carrying tunneling processes involving, respectively, Cooper pairs and the recombination or destruction of Cooper pairs on both sides of the junction. In the adiabatic regime [56], the quasiparticle and the anomalous heat current densities, $\mathcal{P}_{\rm qp}$, $\mathcal{P}_{\cos}$, and $\mathcal{P}_{\sin}$ read, respectively [37,56,57],

$$\mathcal{P}_{\rm qp}(T_1,T_2,V) = \frac{1}{e^2R_aD_2}\int_{-\infty}^{\infty} d\varepsilon \mathcal{N}_1(\varepsilon - eV,T_1) \times \mathcal{N}_2(\varepsilon,T_2)(\varepsilon - eV) \times [f(\varepsilon - eV,T_1) - f(\varepsilon,T_2)], \quad (8)$$

$$\mathcal{P}_{\cos}(T_1,T_2,V) = \frac{1}{e^2R_aD_2}\int_{-\infty}^{\infty} d\varepsilon \mathcal{N}_1(\varepsilon - eV,T_1) \times \mathcal{N}_2(\varepsilon,T_2)\frac{\Delta_1(T_1)\Delta_2(T_2)}{\varepsilon} \times [f(\varepsilon - eV,T_1) - f(\varepsilon,T_2)], \quad (9)$$

$$\mathcal{P}_{\sin}(T_1,T_2,V) = \frac{\rm eV}{2\pi e^2R_aD_2}\iint_{-\infty}^{\infty} d\epsilon_1 d\epsilon_2 \frac{\Delta_1(T_1)\Delta_2(T_2)}{E_2} \times \left(\frac{1 - f(E_1,T_1) - f(E_2,T_2)}{(E_1+E_2)^2 - e^2V^2} + \frac{f(E_1,T_1) - f(E_2,T_2)}{(E_1-E_2)^2 - e^2V^2}\right), \quad (10)$$

where $R_a = RA$ is the resistance per area of the junction, $E_j = \sqrt{\epsilon_j^2 + \Delta_j(T_j)^2}$, $f(E,T) = 1/(1+e^{E/k_BT})$ is the Fermi distribution function, and $\mathcal{N}_j(\varepsilon,T) = \left|{\rm Re}\left[(\varepsilon + i\gamma_j)\Big/\sqrt{(\varepsilon+i\gamma_j)^2 - \Delta_j(T)^2}\right]\right|$ is the reduced superconducting density of state, with $\Delta_j(T_j)$ and γ_j being the BCS energy gap and the Dynes broadening parameter [58] of the jth electrode, respectively.

Interestingly, if we calculate the values of the heat current density $\mathcal{P}_{\rm in}(T_1,T_2,\varphi)$ in the presence of a steady unperturbed soliton, described by Eq. (3) for $u = 0$, an enhancement of $\mathcal{P}_{\rm in}$ centered on the soliton is observed (see Fig. 2, assuming, for simplicity, a homogeneous temperature profile with $T_1 = 7$ K and $T_{\rm bath} = 4.2$ K). Correspondingly, in the presence of a thermal gradient, we expect in the stationary regime a soliton to induce a local warm-up in S_2. The peaked shape of $\mathcal{P}_{\rm in}$ shown in Fig. 2 results from the φ dependence of the anomalous contribution $\mathcal{P}_{\cos}$ in Eq. (7) (notably, the anomalous term $\mathcal{P}_{\sin}$ vanishes in the stationary case; i.e., $\dot\varphi = 0$). In fact, the coefficient $-\cos\varphi$ that is multiplied by the $\mathcal{P}_{\cos}$ term tends to -1 for $\varphi \to \{0, 2\pi\}$, and it is $+1$ for $\varphi = \pi$, namely, corresponding to the center of the soliton. Nevertheless, the quasiparticle contribute $\mathcal{P}_{\rm qp}$ represents a positive offset that still makes $\mathcal{P}_{\rm in}$ positive, so the total heat current flows from the hot to the cold reservoir.

In Eq. (6), the energy exchange between electrons and phonons in the superconductor is accounted for by $\mathcal{P}_{e\text{-ph},2}$, which reads [59]

$$\mathcal{P}_{e\text{-ph},2} = \frac{-\Sigma}{96\zeta(5)k_B^5}\int_{-\infty}^{\infty} dE E\int_{-\infty}^{\infty} d\varepsilon\varepsilon^2{\rm sign}(\varepsilon)M_{E,E+\varepsilon} \times \left\{\coth\left(\frac{\varepsilon}{2k_BT_{\rm bath}}\right)[\mathcal{F}(E,T_2) - \mathcal{F}(E+\varepsilon,T_2)] - \mathcal{F}(E,T_2)\mathcal{F}(E+\varepsilon,T_2) + 1\right\}, \quad (11)$$

where $\mathcal{F}(\varepsilon,T_2) = \tanh(\varepsilon/2k_BT_2)$, $M_{E,E'} = \mathcal{N}_i(E,T_2)\mathcal{N}_i(E',T_2)[1 - \Delta^2(T_2)/(EE')]$, Σ is the electron-phonon

coupling constant, and ζ is the Riemann ζ function. We are assuming that the lattice phonons are very well thermalized with the substrate that resides at $T_{\rm bath}$, thanks to the vanishing Kapitza resistance between thin metallic films and the substrate at low temperatures [33,60].

Going forward in the description of the terms in Eq. (5), $c_v(T) = T\{[d\mathcal{S}(T)]/(dT)]\}$ is the volume-specific heat capacity, with $\mathcal{S}(T)$ being the electronic entropy density of the superconductor S_2 [61,62],

$$\mathcal{S}(T) = -4k_B N_F \int_0^\infty d\varepsilon \mathcal{N}_2(\varepsilon, T) \times \{[1 - f(\varepsilon, T)] \log[1 - f(\varepsilon, T)] + f(\varepsilon, T) \log f(\varepsilon, T)\}. \quad (12)$$

In Eq. (5), $\kappa(T_2)$ is the electronic heat conductivity given by [43]

$$\kappa(T_2) = \frac{\sigma_N}{2e^2 k_B T_2^2} \int_{-\infty}^{\infty} d\varepsilon \varepsilon^2 \frac{\cos^2\{\mathrm{Im}[\mathrm{arctanh}(\frac{\Delta(T_2)}{\varepsilon + i\gamma_2})]\}}{\cosh^2(\frac{\varepsilon}{2k_B T_2})}. \quad (13)$$

In order to comprehensively account for all of the thermal effects, we observe also that the temperature affects both the effective magnetic thickness $t_d(T_1, T_2)$ and the Josephson critical current $I_c(T_1, T_2)$, which varies with the temperatures according to the generalized Ambegaokar and Baratoff formula [63–65]

$$I_c(T_1, T_2) = \frac{1}{2eR} \left| \int_{-\infty}^{\infty} \{f(\varepsilon, T_1)\mathrm{Re}[\mathfrak{F}_1(\varepsilon)]\mathrm{Im}[\mathfrak{F}_2(\varepsilon)] + f(\varepsilon, T_2)\mathrm{Re}[\mathfrak{F}_2(\varepsilon)]\mathrm{Im}[\mathfrak{F}_1(\varepsilon)]\} d\varepsilon \right|, \quad (14)$$

where $\mathfrak{F}_j(\varepsilon) = \Delta_j(T_j)/\sqrt{(\varepsilon + i\gamma_j)^2 - \Delta_j^2(T_j)}$. Accordingly, both the Josephson penetration depth λ_J and the damping parameter α vary with the temperatures; see Fig. 3. Since the soliton width depends on λ_J, this thermal dependence affects both the dynamics and the shape of the soliton and also, then, the temperature profile along the junction.

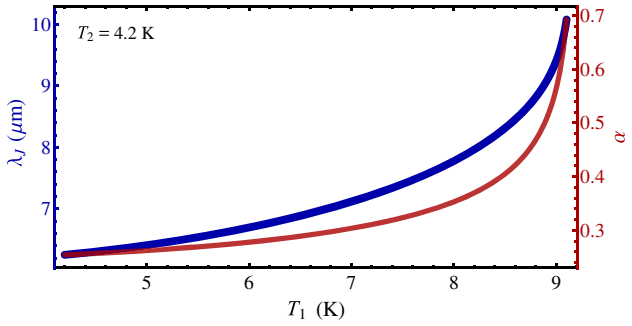

FIG. 3. Josephson penetration length λ_J (left vertical scale, the blue line) and damping parameter α (right vertical scale, the red line) as a function of the temperature of the hot electrode T_1, for $T_2 = 4.2$ K, for a Nb-based LJJ with values of the junction parameters discussed in the text.

The feasibility to affect the soliton dynamics by locally heating the system is the cornerstone of the low-temperature scanning electron microscopy [66–69]. This techniques has proved to be a powerful experimental tool for investigating fluxon dynamics in Josephson devices. The main idea behind this technique is to locally heat a small area (of about a micrometer) of the junction by a narrow electron beam. The generated hot spot acts as a small thermal perturbation with the aim of drastically locally increasing the effective dissipation coefficient. This process results in a change of the I-V characteristic of the device. By gradually scanning the electron beam along the junction surface and measuring the voltage, an "image" of the dynamical state of the LJJ can be produced. Alternatively, in our work, we discuss a sort of thermal imaging of a magnetically excited soliton, through the temperature profile of the floating electrode of the device.

In Fig. 3, we assume a fixed T_2 value since, in the small range of variation of T_2 that we are discussing, the effect of this temperature on λ_J and α is vanishingly small and can therefore be neglected.

Finally, we assume that the electrode S_2 is initially at $T_2(x, 0) = T_{\rm bath}\ \forall\ x \in [0, L]$ and that its ends are thermally isolated, so the boundary conditions of Eq. (5) read $[(\partial T_2)/(\partial x)]|_{x=0,L} = 0$. The choice of the initial temperature of the electrode S_2 is not essential for our discussion since we are assuming that a soliton is excited only when T_2 reaches a steady value $T_{2,s}$ between $T_{\rm bath}$ and T_1.

IV. RESULTS

We consider a $\mathrm{Nb/AlO}_x\mathrm{/Nb}$ S-I-S LJJ characterized by a resistance per area $R_a = 50\ \Omega\mu\mathrm{m}^2$ and a specific capacitance $C_s = 50\ \mathrm{fF}/\mu\mathrm{m}^2$. The linear dimensions of the device are $L = 150\ \mu$m, $W = 0.5\ \mu$m, $D_2 = 0.1\ \mu$m, and $d = 1$ nm. For the Nb electrode, we assume $\lambda_L^0 = 80$ nm, $\sigma_N = 6.7 \times 10^6\ \Omega^{-1}\,\mathrm{m}^{-1}$, $\Sigma = 3 \times 10^9\ \mathrm{W\,m^{-3}\,K^{-5}}$, $N_F = 10^{47}\ \mathrm{J^{-1}\,m^{-3}}$, $\Delta_1(0) = \Delta_2(0) = \Delta = 1.764 k_B T_c$, with $T_c = 9.2$ K being the common critical temperature of the superconductors, and $\gamma_1 = \gamma_2 = 10^{-4}\Delta$.

Here, we focus on the simplest case in which we magnetically excite a soliton, which then moves along the junction as the friction affecting its dynamics stops it. The resulting standing soliton is stable and, if it is far enough to the junction edges and without further perturbations, definitively remains in this position. Then, to model this situation, the "left," i.e., $x = 0$, junction edge is excited by a Gaussian magnetic pulse, with normalized amplitude $\mathcal{H}_{\rm max} = 8.5$ and width $\sigma = 1$ (in units of $[\mu_0/(2\pi)][\Phi_0/(t_d\lambda_J)]$ and ω_p^{-1}, respectively), which induces a soliton moving rightward along the junction. The width and the velocity of the generated soliton directly depend on

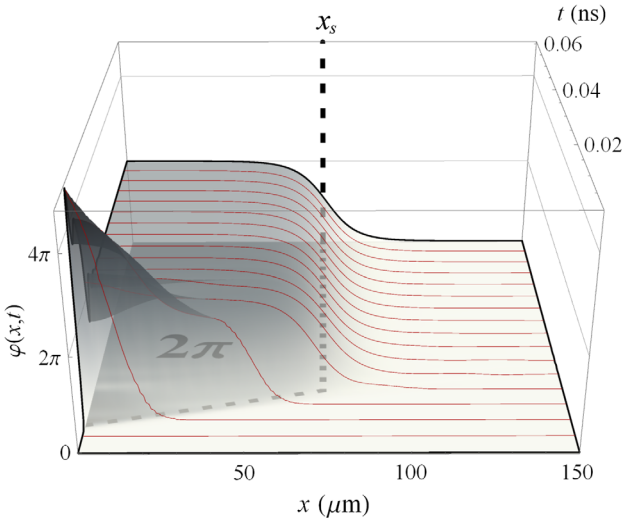

FIG. 4. Phase evolution as a function of the position x and the time t for $T_1 = 7$ K and $T_{\text{bath}} = 4.2$ K. A soliton magnetically excited at $x = 0$ shifts along the junction. Correspondingly, the Josephson phase φ undergoes a 2π step (see the red lines). The phase values and the position x_s of the soliton, which is marked by a black dashed line, are highlighted in the contour plot underneath the main graph.

the temperatures of the system through λ_J and α, respectively. In fact, the higher the temperature, the larger both λ_J and α since both are proportional to $I_c^{-1/2}$ (see Fig. 3). Therefore, by increasing the temperatures, the soliton enlarges and slows down since both λ_J and α increase. This phenomenon shows that the manipulation of the thermal profile along the junction can also be eventually used to modify the soliton dynamics [70].

We impose a thermal gradient across the system, specifically, that the bath resides at $T_{\text{bath}} = 4.2$ K and that S_1 is at a temperature $T_1 = 7$ K kept fixed throughout the computation. The electronic temperature $T_2(x,t)$ of the electrode S_2 is the key quantity for mastering the thermal route across the junction since it floats and can be driven by controlling the soliton along the system.

The evolution of the Josephson phase $\varphi(x,t)$ in the presence of a magnetically excited soliton is shown in Fig. 4. In the figure, a rightward-moving soliton (which corresponds to a 2π step of the phase along the junction) is outlined by red lines at different instants, whereas a dashed line in the contour plot underneath the main graph marks the soliton position. As expected, because of the friction [which is accounted for by a value of the damping parameter $\alpha = (\omega_p RC)^{-1} \simeq 0.3$], the soliton sets in at $x_s \sim 74.8$ μm and definitively stays in that position.

We observe that, corresponding to the soliton, the heat flux P_{in} is clearly enhanced [see Fig. 5(a)]. Specifically, the steady value of the heat current corresponding to the soliton is $P_{\text{in}} \sim 1.1$ μW, whereas it is $P_{\text{in}} \sim 0.3$ μW elsewhere.

Finally, the behavior of the temperature $T_2(x,t)$ reflects the behavior of the thermal flux P_{in}, as is shown in Fig. 5(b). In this case, the soliton is excited after about 2 ns, namely, as the whole electrode S_2 is thermalized at the steady "unperturbed" (i.e., unaffected by excitations) temperature $T_{2,s} \simeq 4.23$ K. Interestingly, the soliton induces a local intense warm-up in S_2, with a steady maximum temperature $T_{2,\text{max}} \simeq 4.29$ K.

We observe that, as the soliton sets in at x_s, the temperature enhances exponentially, approaching its steady value; see Fig. 5(b). The thermal response time can be estimate as the characteristic time of the exponential

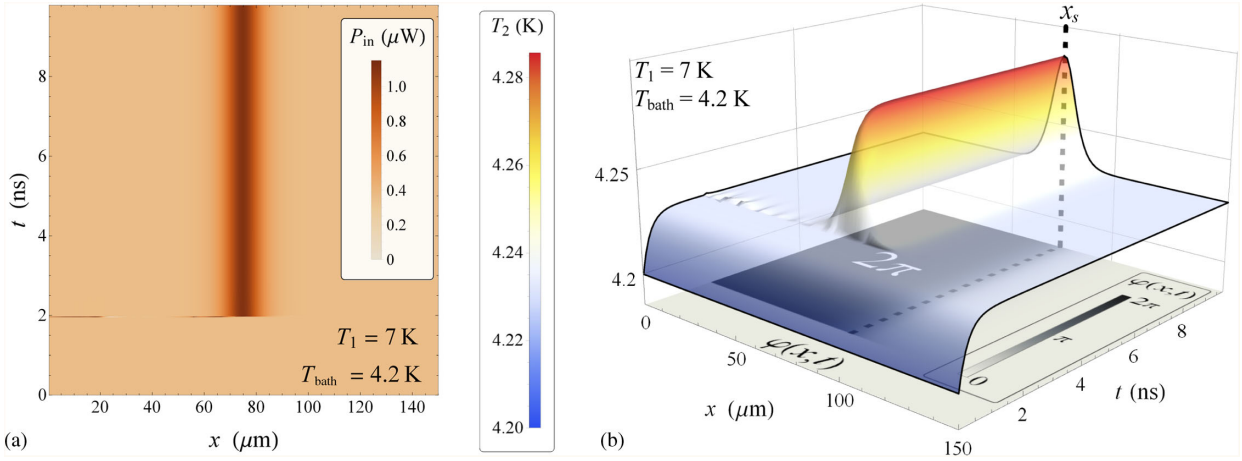

FIG. 5. (a) Heat current $P_{\text{in}}(T_1, T_2, \varphi, V)$ flowing from S_1 to S_2; see Eq. (7). (b) Evolution of the temperature $T_2(x,t)$ of S_2. In both panels, the soliton is magnetically excited to the left end, i.e., $x = 0$, after approximately 2 ns. At this time, the superconducting electrode S_2 is already fully thermalized at the steady temperature $T_{2,s} \sim 4.23$ K. Then, corresponding to the induced soliton, we observe a clear enhancement of both P_{in} and T_2. In (b), the phase values $\varphi(x,t)$ and the position of the soliton, which is marked by a black dashed line, are highlighted in the contour plot underneath the main graph. For both panels, $T_1 = 7$ K, $T_{\text{bath}} = 4.2$ K, and the junction is initially at the temperature $T_2(x,0) = T_{\text{bath}}$ $\forall$ $x \in [0 - L]$.

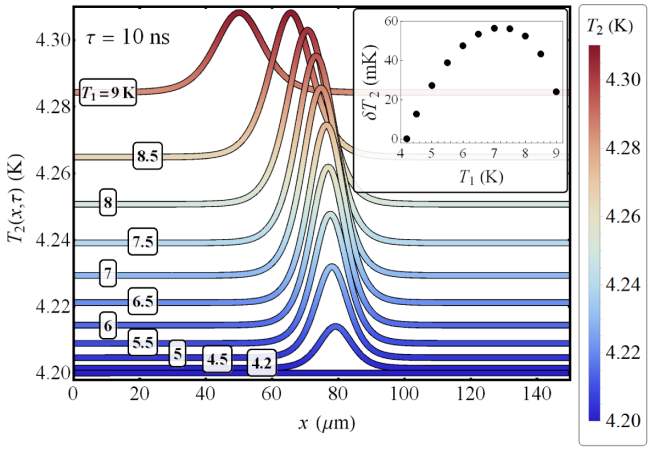

FIG. 6. Temperature $T_2(x,\tau)$ at $\tau = 10$ ns for a few values of T_1. (Inset) The T_2 modulation amplitude, δT_2, as a function of T_1. The bath temperature is $T_{\text{bath}} = 4.2$ K and the junction is initially at the temperature $T_2(x,0) = T_{\text{bath}}\ \forall\ x \in [0-L]$.

evolution by which the temperature approaches its stationary value. Then, from Fig. 5(b), we deduce the value $\tau_{\text{th}} \sim 0.25$ ns. Markedly, a very good estimate of this thermal response time results also in a linear response regime, namely, by first order expanding the heat current terms in Eq. (5). In fact, by following the same procedure developed in Ref. [46], we obtain a thermal switching time $\tau_{\text{sw}} \simeq 0.1$ ns.

The role of the temperature T_1 is illustrated in Fig. 6, where $T_2(x,\tau)$ is calculated at $\tau = 10$ ns at a few values of T_1 and $T_{\text{bath}} = 4.2$ K. By increasing T_1, the temperature peak shifts leftward and becomes wider, simply because the soliton slows down and enlarges, as a consequence of the parameter variations discussed in Fig. 3. Interestingly, the T_2 modulation amplitude, $\delta T_2 = T_{2,\max} - T_{2,s}$—defined as the difference between the maximum and minimum values of $T_2(x,\tau)$ along the junction at a fixed time τ—behaves nonmonotonically by varying T_1 (see the inset of Fig. 6). In fact, δT_2 vanishes for low T_1 values (specifically, for $T_1 = T_{\text{bath}}$, there is no thermal gradient across the system). It then increases up to $\delta T_2 \sim 56$ mK for $T_1 = 7$ K, and it finally reduces again for $T_1 \to T_c$ due to the temperature-induced suppression of the energy gaps in the superconductors.

The physical effect we describe here can promptly find an application as a Josephson thermal router [36]. Specifically, we can design a setup in which we direct the heat through a soliton to a superconducting finger electrode, attached, for instance, to x_s, in order to selectively warm it up. Additionally, this idea can be improved further by including an external electric bias current across the junction. In fact, a bias current density, J_b, acts on the soliton with a Lorentz force, $\mathbf{F}_L = \mathbf{J}_b \times \mathbf{\Phi}_0$ (with the direction of $\mathbf{\Phi}_0$ depending on the polarity of the soliton). So, in the presence of an external bias current, according to the perturbational approach [5], a soliton drifts with a velocity approximately given by $u_d = 1/\sqrt{1 + [4\alpha/(\pi\gamma)]^2}$ [4], with $\gamma = J_b/J_c$—specifically, for a low bias current $u_d \simeq [(\pi\gamma)/(4\alpha)]$. This behavior allows us to actively control the dynamics and the final position of the soliton, and thus the local temperature of the electrode. Therefore, a multiterminal device allowing us to distribute the heat among several reservoirs can be conceived of, in which we can select which terminal to heat by shifting the soliton along the junction through the bias current. Clearly, the time-dependent approach we illustrate in this paper is indispensable for accurately describing the dynamical temperature response when the soliton moves from one finger to the next one, and then for properly mastering the operating principles of a multiterminal device.

V. CONCLUSIONS

In conclusion, we discuss in this paper the phase-coherent thermal transport in a temperature-biased LJJ, where the thermal conduction across the system can be controlled through solitonic excitations. Specifically, we analyze the evolution of the temperature T_2 of the floating "cold" electrode of the junction, as the temperature T_1 of the "hot" electrode is kept fixed and the thermal contact with a phonon bath is taken into account. Specifically, corresponding to a magnetically excited soliton, we observe a clear enhancement of the heat current P_{in} flowing through the junction. Correspondingly, a soliton-induced temperature peak occurs, with a height of up to $\delta T_2 \sim 56$ mK in the realistic Nb-based proposed setup.

Finally, the physical properties of the device depend on the evolution of the superconducting order parameter along the junction and, hence, on the dynamics of solitons which can be accurately controlled by the external magnetic field, bias current, and shape engineering. This flexibility will make it possible to suggest alternative caloritronics applications enabling, for instance, the handling of the local thermal transport at specific points of the junction, i.e., a solitonic thermal router. The analysis also shows the possibility of affecting the solitonic properties by manipulating the thermal profile, increasing the possible interplay between thermal and solitonic dynamics. Additionally, the solitonic nature of the system ensures protection against environmental disturbances and a highly controllable, unaffected by noise, heat flow. The results obtained will clarify the interplay between solitons and caloritronics at nanoscale, paving the way for the realization of alternative coherent devices based on soliton-sustained thermal transport.

Moreover, this device could represent the link between two recent proposals concerning a Josephson-based, phase-tunable thermal logic [71] and a logic using fluxons in LJJs [72].

The suggested systems could be implemented by standard nanofabrication techniques through the setup used, for instance, for the short JJ-based thermal diffractor [41]. The

modulations of the temperature of the drain cold electrode is usually obtained by realizing a Josephson junction with a large superconducting electrode, whose temperature is blocked at a fixed value, and a small electrode with a small thermal capacity. In this way, the heat transferred significantly affects the temperature of the latter electrode, which is then measured.

ACKNOWLEDGMENTS

C. G. and F. G. acknowledge the European Research Council under the European Union's Seventh Framework Program (FP7/ERC Grant Agreement No. 615187-COMANCHE for the partial financial support. P. S. has received funding from the European Union FP7 under REA Grant Agreement No. 630925–COHEAT and from MIUR-FIRB Project Coca (Grant No. RBFR1379UX). A. B. acknowledges the support of the Italian MIUR-FIRB program via the HybridNanoDev project, under Grant No. RBFR1236VV, and the CNR-CONICET cooperation program "Energy conversion in quantum nanoscale hybrid devices."

[1] A. Scott, M. P. Sørensen, and P. L. Christiansen, *Nonlinear Science: Emergence and Dynamics of Coherent Structures*, Oxford Texts in Applied and Engineering Mathematics Vol. 8 (Oxford University Press, New York, 1999).

[2] T. Dauxois and M. Peyrard, *Physics of Solitons* (Cambridge University Press, Cambridge, England, 2006).

[3] R. D. Parmentier, in *The New Superconducting Electronics*, edited by Harold Weinstock and Richard W. Ralston (Springer, Dordrecht, 1993), p. 221.

[4] A. V. Ustinov, Solitons in Josephson junctions, Physica (Amsterdam) **123D**, 315 (1998).

[5] D. W. McLaughlin and A. C. Scott, Perturbation analysis of fluxon dynamics, Phys. Rev. A **18**, 1652 (1978).

[6] A. C. Scott and W. J. Johnson, Internal flux motion in large Josephson junctions, Appl. Phys. Lett. **14**, 316 (1969).

[7] T. A. Fulton and R. C. Dynes, Single vortex propagation in Josephson tunnel junctions, Solid State Commun. **12**, 57 (1973).

[8] S. Ooi, Sergey Savel'ev, M. B. Gaifullin, T. Mochiku, K. Hirata, and Franco Nori, Nonlinear Nanodevices Using Magnetic Flux Quanta, Phys. Rev. Lett. **99**, 207003 (2007).

[9] D. R. Gulevich and F. V. Kusmartsev, New phenomena in long Josephson junctions, Supercond. Sci. Technol. **20**, S60 (2007).

[10] S. Anders *et al.*, European roadmap on superconductive electronics—Status and perspectives, Physica (Amsterdam) **470C**, 2079 (2010).

[11] K. K. Likharev, Superconductor digital electronics, Physica (Amsterdam) **482C**, 6 (2012).

[12] R. Monaco, Magnetic sensors based on long Josephson tunnel junctions, Supercond. Sci. Technol. **25**, 115011 (2012).

[13] C. Guarcello, D. Valenti, G. Augello, and B. Spagnolo, The role of non-Gaussian sources in the transient dynamics of long Josephson junctions, Acta Phys. Pol. B **44**, 997 (2013).

[14] R. Monaco, C. Granata, R. Russo, and A. Vettoliere, Ultra-low-noise magnetic sensing with long Josephson tunnel junctions, Supercond. Sci. Technol. **26**, 125005 (2013).

[15] C. Granata, A. Vettoliere, and R. Monaco, Noise performance of superconductive magnetometers based on long Josephson tunnel junctions, Supercond. Sci. Technol. **27**, 095003 (2014).

[16] *The Sine-Gordon Model and Its Applications: From Pendula and Josephson Junctions to Gravity and High-Energy Physics*, edited by J. Cuevas-Maraver, P. G. Kevrekidis, and F. Williams, Nonlinear Systems and Complexity (Springer, New York, 2014).

[17] V. P. Koshelets, Sub-terahertz sound excitation and detection by a long Josephson junction, Supercond. Sci. Technol. **27**, 065010 (2014).

[18] D. Valenti, C. Guarcello, and B. Spagnolo, Switching times in long-overlap Josephson junctions subject to thermal fluctuations and non-Gaussian noise sources, Phys. Rev. B **89**, 214510 (2014).

[19] I. I. Soloviev, N. V. Klenov, A. L. Pankratov, L. S. Revin, E. Il'ichev, and L. S. Kuzmin, Soliton scattering as a measurement tool for weak signals, Phys. Rev. B **92**, 014516 (2015).

[20] C. Guarcello, D. Valenti, A. Carollo, and B. Spagnolo, Stabilization effects of dichotomous noise on the lifetime of the superconducting state in a long Josephson junction, Entropy **17**, 2862 (2015).

[21] A. Vettoliere, C. Granata, and R. Monaco, Long Josephson junction in ultralow-noise magnetometer configuration, IEEE Trans. Magn. **51**, 1 (2015).

[22] A. L. Pankratov, K. G. Fedorov, M. Salerno, S. V. Shitov, and A. V. Ustinov, Nonreciprocal transmission of microwaves through a long Josephson junction, Phys. Rev. B **92**, 104501 (2015).

[23] C. Guarcello, D. Valenti, A. Carollo, and B. Spagnolo, Effects of Lévy noise on the dynamics of sine-Gordon solitons in long Josephson junctions, J. Stat. Mech. (2016) 054012.

[24] I. A. Golovchanskiy, N. N. Abramov, V. S. Stolyarov, O. V. Emelyanova, A. A. Golubov, A. V. Ustinov, and V. V. Ryazanov, Ferromagnetic resonance with long Josephson junction, Supercond. Sci. Technol. **30**, 054005 (2017).

[25] C. Guarcello, P. Solinas, M. Di Ventra, and F. Giazotto, Solitonic Josephson-based meminductive systems, Sci. Rep. **7**, 46736 (2017).

[26] D. Hill, S. K. Kim, and Y. Tserkovnyak, Easy-plane magnetic strip as a long Josephson junction, arXiv:1802.04229.

[27] E. Goldobin, A. Sterck, and D. Koelle, Josephson vortex in a ratchet potential: Theory, Phys. Rev. E **63**, 031111 (2001).

[28] G. Carapella, G. Costabile, N. Martucciello, M. Cirillo, R. Latempa, A. Polcari, and G. Filatrella, Experimental realization of a relativistic fluxon ratchet, Physica (Amsterdam) **382C**, 337 (2002).

[29] G. Carapella, N. Martucciello, and G. Costabile, Experimental investigation of flux motion in exponentially shaped Josephson junctions, Phys. Rev. B **66**, 134531 (2002).

[30] T. Dobrowolski, Kink motion in a curved Josephson junction, Phys. Rev. E **79**, 046601 (2009).
[31] A. V. Ustinov, in *Nonlinear Superconductive Electronics and Josephson Devices*, edited by Giovanni Costabile, Sergio Pagano, Niels Falsig Pedersen, and Maurizio Russo (Springer, Boston, 1991), p. 315.
[32] R. Fehrenbacher, V. B. Geshkenbein, and G. Blatter, Pinning phenomena and critical currents in disordered long Josephson junctions, Phys. Rev. B **45**, 5450 (1992).
[33] F. Giazotto, T. T. Heikkilä, A. Luukanen, A. M. Savin, and Jukka P. Pekola, Opportunities for mesoscopics in thermometry and refrigeration: Physics and applications, Rev. Mod. Phys. **78**, 217 (2006).
[34] M. J. Martínez-Pérez, P. Solinas, and F. Giazotto, Coherent caloritronics in Josephson-based nanocircuits, J. Low Temp. Phys. **175**, 813 (2014).
[35] A. Fornieri and F. Giazotto, Towards phase-coherent caloritronics in superconducting circuits, Nat. Nanotechnol. **12**, 944 (2017).
[36] G. Timossi, A. Fornieri, F. Paolucci, C. Puglia, and F. Giazotto, Phase-tunable Josephson thermal router, Nano Lett., DOI: 10.1021/acs.nanolett.7b04906 (2018).
[37] K. Maki and A. Griffin, Entropy Transport between Two Superconductors by Electron Tunneling, Phys. Rev. Lett. **15**, 921 (1965).
[38] F. Giazotto and M. J. Martínez-Pérez, Phase-controlled superconducting heat-flux quantum modulator, Appl. Phys. Lett. **101**, 102601 (2012).
[39] F. Giazotto and M. J. Martínez-Pérez, The Josephson heat interferometer, Nature (London) **492**, 401 (2012).
[40] F. Giazotto, M. J. Martínez-Pérez, and P. Solinas, Coherent diffraction of thermal currents in Josephson tunnel junctions, Phys. Rev. B **88**, 094506 (2013).
[41] M. J. Martínez-Pérez and F. Giazotto, A quantum diffractor for thermal flux, Nat. Commun. **5**, 3579 (2014).
[42] A. Fornieri, C. Blanc, R. Bosisio, S. D'Ambrosio, and F. Giazotto, Nanoscale phase engineering of thermal transport with a Josephson heat modulator, Nat. Nanotechnol. **11**, 258 (2016).
[43] A. Fornieri, G. Timossi, P. Virtanen, P. Solinas, and F. Giazotto, 0-π phase-controllable thermal Josephson junction, Nat. Nanotechnol. **12**, 425 (2017).
[44] C. Guarcello, F. Giazotto, and P. Solinas, Coherent diffraction of thermal currents in long Josephson tunnel junctions, Phys. Rev. B **94**, 054522 (2016).
[45] C. Guarcello, P. Solinas, M. Di Ventra, and F. Giazotto, Hysteretic Superconducting Heat-Flux Quantum Modulator, Phys. Rev. Applied **7**, 044021 (2017).
[46] C. Guarcello, P. Solinas, A. Braggio, M. Di Ventra, and F. Giazotto, Josephson Thermal Memory, Phys. Rev. Applied **9**, 014021 (2018).
[47] A. R. Bishop, J. A. Krumhansl, and S. E. Trullinger, Solitons in condensed matter: A paradigm, Physica (Amsterdam) **1D**, 1 (1980).
[48] A. Barone and G. Paternò, *Physics and Applications of the Josephson Effect* (Wiley, New York, 1982).
[49] P. S. Lomdahl, O. H. Soerensen, and P. L. Christiansen, Soliton excitations in Josephson tunnel junctions, Phys. Rev. B **25**, 5737 (1982).
[50] N. Grønbech-Jensen, Zero-voltage states in ac-driven long Josephson junctions, Phys. Rev. B **45**, 7315 (1992).
[51] A. Davidson, B. Dueholm, and N. F. Pedersen, Experiments on soliton motion in annular Josephson junctions, J. Appl. Phys. **60**, 1447 (1986).
[52] A. V. Ustinov, T. Doderer, R. P. Huebener, N. F. Pedersen, B. Mayer, and V. A. Oboznov, Dynamics of Sine-Gordon Solitons in the Annular Josephson Junction, Phys. Rev. Lett. **69**, 1815 (1992).
[53] A. V. Ustinov, Fluxon insertion into annular Josephson junctions, Appl. Phys. Lett. **80**, 3153 (2002).
[54] S. B. Kaplan, C. C. Chi, D. N. Langenberg, J. J. Chang, S. Jafarey, and D. J. Scalapino, Quasiparticle and phonon lifetimes in superconductors, Phys. Rev. B **14**, 4854 (1976).
[55] B. Frank and W. Krech, Electronic cooling in superconducting tunnel junctions, Phys. Lett. A **235**, 281 (1997).
[56] D. Golubev, T. Faivre, and J. P. Pekola, Heat transport through a Josephson junction, Phys. Rev. B **87**, 094522 (2013).
[57] P. Virtanen, P. Solinas, and F. Giazotto, Spectral representation of the heat current in a driven Josephson junction, Phys. Rev. B **95**, 144512 (2017).
[58] R. C. Dynes, V. Narayanamurti, and J. P. Garno, Direct Measurement of Quasiparticle-Lifetime Broadening in a Strong-Coupled Superconductor, Phys. Rev. Lett. **41**, 1509 (1978).
[59] A. V. Timofeev, C. P. García, N. B. Kopnin, A. M. Savin, M. Meschke, F. Giazotto, and J. P. Pekola, Recombination-Limited Energy Relaxation in a Bardeen-Cooper-Schrieffer Superconductor, Phys. Rev. Lett. **102**, 017003 (2009).
[60] F. C. Wellstood, C. Urbina, and John Clarke, Hot-electron effects in metals, Phys. Rev. B **49**, 5942 (1994).
[61] H. Rabani, F. Taddei, O. Bourgeois, R. Fazio, and F. Giazotto, Phase-dependent electronic specific heat of mesoscopic Josephson junctions, Phys. Rev. B **78**, 012503 (2008).
[62] P. Solinas, R. Bosisio, and F. Giazotto, Microwave quantum refrigeration based on the Josephson effect, Phys. Rev. B **93**, 224521 (2016).
[63] F. Giazotto and J. P. Pekola, Josephson tunnel junction controlled by quasiparticle injection, J. Appl. Phys. **97**, 023908 (2005).
[64] S. Tirelli, A. M. Savin, C. P. Garcia, J. P. Pekola, F. Beltram, and F. Giazotto, Manipulation and Generation of Supercurrent in Out-of-Equilibrium Josephson Tunnel Nanojunctions, Phys. Rev. Lett. **101**, 077004 (2008).
[65] R. Bosisio, P. Solinas, A. Braggio, and F. Giazotto, Photonic heat conduction in Josephson-coupled Bardeen-Cooper-Schrieffer superconductors, Phys. Rev. B **93**, 144512 (2016).
[66] S. G. Lachenmann, T. Doderer, R. P. Huebener, D. Quenter, J. Niemeyer, and R. Pöpel, Spatially resolved study of the dynamics of Josephson tunnel junctions, Phys. Rev. B **48**, 3295 (1993).
[67] R. Gross and D. Koelle, Low temperature scanning electron microscopy of superconducting thin films and Josephson junctions, Rep. Prog. Phys. **57**, 651 (1994).

[68] B. A. Malomed and A. V. Ustinov, Analysis of testing the single-fluxon dynamics in a long Josephson junction by a dissipative spot, Phys. Rev. B **49**, 13024 (1994).

[69] T. Doderer, Microscopic imaging of Josephson junction dynamics, Int. J. Mod. Phys. B **11**, 1979 (1997).

[70] V. M. Krasnov, V. A. Oboznov, and N. F. Pedersen, Fluxon dynamics in long Josephson junctions in the presence of a temperature gradient or spatial nonuniformity, Phys. Rev. B **55**, 14486 (1997).

[71] F. Paolucci, G. Marchegiani, E. Strambini, and F. Giazotto, Phase-tunable thermal logic: Computation with heat, arXiv:1709.08609.

[72] W. Wustmann and K. D. Osborn, One- and two-bit reversible fluxon logic gates, arXiv:1711.04339.